The bacterial tyrosine kinase system CpsBCD governs the length of capsule polymers

Rei Nakamoto[a], Jeric Mun Chung Kwan[b], Jasmine Fei Li Chin[c], Hui Ting Ong[c], Josue Flores-Kim[d], Caroline Midonet[d], Michael S. VanNieuwenhze[e], Xue Li Guan[b], and Lok-To Sham[a,1]

[a]Infectious Diseases Translational Research Programme, Department of Microbiology and Immunology, Yong Loo Lin School of Medicine, National University of Singapore, Singapore 117545; [b]Lee Kong Chian School of Medicine, Nanyang Technological University, Singapore 308232; [c]Mechanobiology Institute, National University of Singapore 117411, Singapore; [d]Department of Microbiology and Immunobiology, Harvard Medical School, Boston, MA 02115; and [e]Department of Molecular and Cellular Biochemistry, Indiana University, Bloomington, IN 47405

Edited by Staffan Normark, Karolinska Institutet, Stockholm, Sweden, and approved September 16, 2021 (received for review February 25, 2021)

Many pathogenic bacteria are encased in a layer of capsular polysaccharide (CPS). This layer is important for virulence by masking surface antigens, preventing opsonophagocytosis, and avoiding mucus entrapment. The bacterial tyrosine kinase (BY-kinase) regulates capsule synthesis and helps bacterial pathogens to survive different host niches. BY-kinases autophosphorylate at the C-terminal tyrosine residues upon external stimuli, but the role of phosphorylation is still unclear. Here, we report that the BY-kinase CpsCD is required for growth in *Streptococcus pneumoniae*. Cells lacking a functional *cpsC* or *cpsD* accumulated low molecular weight CPS and lysed because of the lethal sequestration of the lipid carrier undecaprenyl phosphate, resulting in inhibition of peptidoglycan (PG) synthesis. CpsC interacts with CpsD and the polymerase CpsH. CpsD phosphorylation reduces the length of CPS polymers presumably by controlling the activity of CpsC. Finally, pulse–chase experiments reveal the spatiotemporal coordination between CPS and PG synthesis. This coordination is dependent on CpsC and CpsD. Together, our study provides evidence that BY-kinases regulate capsule polymer length by fine-tuning CpsC activity through autophosphorylation.

Streptococcus pneumoniae | capsular polysaccharide | bacterial tyrosine kinase

The respiratory pathogen *Streptococcus pneumoniae*(pneumococcus) was estimated to cause 197 million cases of lower respiratory tract infections globally in 2016, which ultimately led to 1.1 million deaths (1). The success of *S. pneumoniae* as a human pathogen is partly attributed to the capsular polysaccharide (CPS) covering its cell surface (2, 3). This carbohydrate layer protects the bacterial cell from a variety of host insults, such as complement deposition, opsonophagocytosis, mucus entrapment, and neutrophil extracellular traps (reviewed in refs. 2–5). CPS is also important for the colonization of the nasal cavity (6). Since antibodies against pneumococcal proteins presumably are unable to penetrate the CPS barrier (7), the host responds by synthesizing anti-CPS antibodies, which agglutinate pneumococci at the nasopharyngeal mucosa and facilitate mucociliary clearance (8). Anti-CPS antibodies also inhibit the proliferation of invaded bacteria in the bloodstream. This forms the basis of the vaccine strategy against *S. pneumoniae*. All licensed pneumococcal vaccines target the CPS. Despite their effectiveness, these vaccines can cover only a small number of serotypes because of the heterogenicity of the CPS structure. For example, there are at least 100 known serotypes identified in *S. pneumoniae* (9), and the broadest spectrum vaccine covers 23 of them (10). CPS-based vaccines are therefore prone to the increasing problem of serotype replacement (11) and cannot provide complete protection (10).

Most of the pneumococcal CPS are produced via the Wzx/Wzy pathway (2–4). In this pathway, CPS genes are organized into an operon, and its expression is driven by a single P_{cps} promoter (12). The first four genes, *cpsABCD*, are widely conserved, but their functions are not fully understood. *cpsA* encodes a LytR-Cps2A-Psr (LCP) protein, which is thought to conjugate CPS to peptidoglycan (PG) (13). Unlike in *Staphylococcus aureus* (14, 15) and *Streptococcus agala*ctiae (16), deletion of *cpsA* in *S. pneumoniae* does not have any detectable effect on CPS production or attachment (17). CpsBCD constitutes a phosphoregulatory system that has been implicated in regulating CPS production. Immediately downstream are the serotype-specific genes encoding the initiating phosphoglycosyl transferase (PGT; *cpsE* in serotype 2) and other late-stage enzymes such as the flippase (*cpsJ*), the polymerase (*cpsH*), glycosyltransferases (GTs), and acetyltransferases (2–5).

The serotype 2 CPS pathway begins with the addition of a glucose residue to the undecaprenyl phosphate (Und-P) lipid carrier by CpsE. Other sugars are sequentially assembled on the glycosylated Und-P to form a repeating unit, which is then flipped, polymerized, and attached to PG (2–5, 18) (Fig. 1). Und-P is not abundant in *S. pneumoniae* (19) and is shared with the PG synthesis pathway (20). Thus, premature termination of the CPS pathway by inactivating any of the late-stage enzymes is lethal, as it results in the accumulation of dead-end intermediates and sequesters Und-P. The lethality can be alleviated by suppressor mutations in *cpsE*, which restores growth by preventing Und-P from entering the CPS pathway (21, 22).

The level of CPS is presumably regulated at different stages of infection (23). This is especially important during the early

Significance

Controlling the length of capsular polysaccharide (CPS) chains is thought to promote pathogen survival in various host niches. The polysaccharide copolymerase 2b family proteins were implicated in regulating CPS sizes. These proteins form a bacterial tyrosine kinase (BY-kinase) system that responds to the environment by modulating its phosphorylation status. Nevertheless, the role of autophosphorylation in capsule synthesis is still elusive. Here, we found that the disruption of BY-kinase CpsCD is lethal in *Streptococcus pneumoniae* serotype 2 strain D39. Phosphorylation of CpsD resulted in shorter CPS polymers. We also provide cell biology evidence that CPS synthesis is coordinated with peptidoglycan synthesis.

Author contributions: R.N. and L.-T.S. designed research; R.N., J.M.C.K., J.F.L.C., J.F.-K., C.M., and X.L.G. performed research; M.S.V. contributed new reagents/analytic tools; R.N., J.M.C.K., H.T.O., X.L.G., and L.-T.S. analyzed data; and R.N. and L.-T.S. wrote the paper.

The authors declare no competing interest.

This article is a PNAS Direct Submission.

[1]To whom correspondence may be addressed. Email: lsham@nus.edu.sg.

This article contains supporting information online at http://www.pnas.org/lookup/suppl/doi:10.1073/pnas.2103377118/-/DCSupplemental.

Published November 3, 2021.

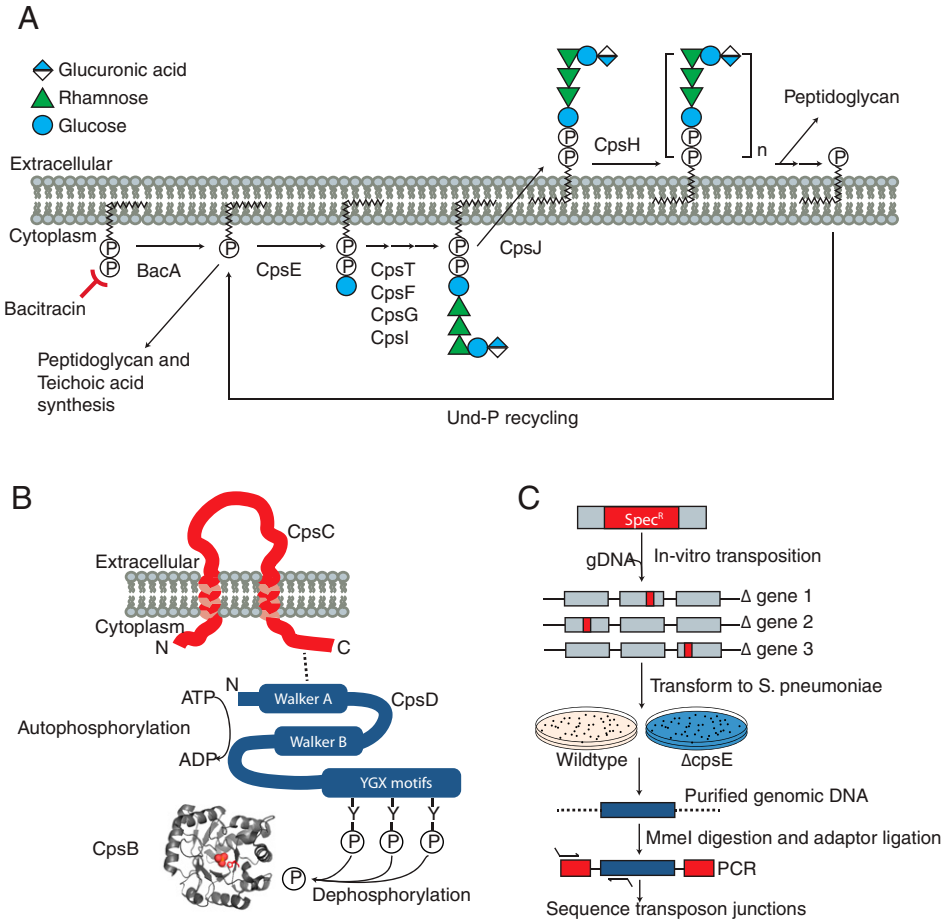

Fig. 1. The serotype 2 CPS synthesis pathway of *S. pneumoniae*. (*A*) CPS is built by installing sugars sequentially on the Und-P lipid carrier in the cytoplasm. The lipid-linked precursor is flipped, polymerized, and transferred to the PG by a yet-to-be-identified ligase. Und-P is then recycled after dephosphorylation for the next round of CPS synthesis. (*B*) Graphical representation of phosphoregulatory system in *S. pneumoniae*. CpsC has a large extracellular loop that structurally resembles Wzz. It interacts with CpsD and recruits it to the septal region through its C-terminal domain. CpsD autophosphorylates at the three C-terminal tyrosine residues that presumably modulate CpsCD activity. CpsB (Protein Data Bank: 2wjf) is a manganese-dependent phosphatase that dephosphorylates CpsD~P. The residue highlighted in red is the catalytic histidine (His136), which is in close proximity to the leaving phosphate group. (*C*) Outline of the Tn-seq screen. Pneumococcal genomic DNA was transposon mutagenized and transformed into the wild-type and Δ*cpsE* strains. Survivors were pooled, and the genomic DNA was extracted. Transposons (represented by blue boxes) were mapped by MmeI digestion, adapter ligation, PCR, and next-generation sequencing.

phase of infection because the CPS may block the underlying adhesion factors. At least three mechanisms that control CPS level have been proposed: transcriptional regulation by the P_{cps} promoter (12, 24), epigenetic regulation by phase variation (25–27), and posttranslational regulation by the bacterial tyrosine kinase (BY-kinase) system CpsBCD (28–30). The CpsBCD complex structurally resembles Wzc in gram-negative bacteria, which consists of a transmembrane protein CpsC, a cytoplasmic kinase CpsD, and a polymerase and histidinol phosphatase CpsB (Fig. 1) (29). CpsD phosphorylates its C-terminal tyrosine residues in response to external stimuli like oxygen (29). The C-terminal domain of CpsC stabilizes CpsD and recruits it to the division septum (28). It is also required for the autokinase activity of CpsD (17). CpsB dephosphorylates CpsD and perhaps other CpsD targets to complete the phosphorylation cycle (17, 28). Nevertheless, the CpsB phosphatase activity appears to be dispensable for capsule production or regulation (29). The CpsBCD system may coordinate CPS synthesis, primarily because deletion of CpsC led to the delocalization of CPS proteins and the loss of CPS synthesis in the septal region (28, 30). The serine/threonine kinase PknB (StkP in *S. pneumoniae*) has been implicated in the coordination of CPS and PG synthesis (31). However, how these two processes tied together, especially in response to the changing environment, is still largely unknown.

Deletions and point mutations of *cpsB*, *cpsC*, and *cpsD* resulted in conflicting phenotypes that have not yet been reconciled (summarized in *SI Appendix*, Table S1). The discrepancy may be due to differences in the genetic background and/or growth conditions. Likewise, the role of CpsD autophosphorylation in regulating CPS synthesis is not fully understood. In this study, we found that the CpsCD system in *S. pneumoniae* is required for growth. Lethality caused by deletion of *cpsC* or *cpsD* could be suppressed by mutations in *cpsE*. Once we accounted for the essentiality of CpsCD, we revealed that CpsD phosphorylation reduces the size of the CPS polymers. We identified the residues in the extracellular loop of CpsC that are required for the production of long polymers, providing insights into the possible copolymerase activity. In addition, CpsC and CpsD are required to organize the CPS complex such that CPS synthesis is spatiotemporally coordinated with PG synthesis. The loss of CpsCD activity will result in lethal sequestration of Und-P and halt PG synthesis.

Results

Transposon Sequencing Identified Factors Required for CPS Synthesis. We performed transposon sequencing (Tn-seq) (32) on two mutant libraries prepared from the wild-type serotype 2 strain D39 and its isogenic Δ*cpsE* strain to identify factors required for CPS synthesis. The rationale is that deletion of *cpsE* will render factors required for the latter steps of CPS synthesis dispensable (21). Thus, the frequencies from which we recovered the transposon mutations that inactivated these factors would increase in the Δ*cpsE* background compared to the wild-type cells (Fig. 1). As expected, the late CPS enzymes (e.g., *cpsF*, *cpsG*, *cpsI*, *cpsJ*, *cpsH*, and *cpsK*) (17, 21) as well as the Mg^{2+} importer *mgtA* (33) were found to be essential for growth only in the wild-type strain (*SI Appendix*, Table S2 and Dataset S1). Surprisingly, we also observed significantly fewer transposon insertions in *cpsC* in the wild-type background. To validate this hit, we attempted to reconstruct the Δ*cpsC* mutant

in the wild-type and Δ*cpsE* strains. No colony was observed when *cpsC* was disrupted by an antibiotic cassette (Δ*cpsC*::P-*erm*) in the wild-type background, whereas hundreds of transformants were obtained if the recipient strain was the Δ*cpsE* mutant. The requirement of *cpsC* for growth appeared not to be serotype or genotype dependent because viable Δ*cpsC* transformants could not be recovered in the serotype 4 strain TIGR4 and an isogenic capsule-switch variant of serotype 19F (*SI Appendix*, Table S3).

CpsC and CpsD Are Essential for Growth in Serotype 2 Strain D39. To determine the phenotype of the Δ*cpsC* mutant, we constructed strain NUS0267 [Δ*cpsE*//P_{Zn}-*cpsE*] in which the expression of *cpsE* is under the control of a zinc-inducible promoter. The supplementation of Zn^{2+} to the medium did not affect the production of CPS or reduce the growth rate of the wild-type and Δ*cpsE* strains (*SI Appendix*, Fig. S1). CPS was produced at a comparable level when Zn^{2+} was added to the culture of strain NUS0267 [Δ*cpsE*//P_{Zn}-*cpsE*] (*SI Appendix*, Figs. S1 and S2). Next, we constructed markerless deletion mutants of *cpsC* and *cpsD* in the Δ*cpsE*//P_{Zn}-*cpsE* background. Disruption of *cpsC* or *cpsD* was lethal when *cpsE* was induced (Fig. 2 and *SI Appendix*, Table S4). Growth was arrested approximately 2 h after Zn^{2+} addition with a concomitant reduction in plating efficiency (*SI Appendix*, Fig. S3). Interestingly, phenotypes of the Δ*cpsC* and Δ*cpsD* mutants were affected by the growth media. The growth defects were less evident when the cells were grown in brain heart infusion (BHI) broth compared to BHI plates and tryptic soy broth (TSB) (*SI Appendix*, Fig. S4), and we have not yet uncovered the mechanism behind the phenotype variation. Thus, we selected TSB in our subsequent experiments to study the lethality of Δ*cpsC* and Δ*cpsD* mutations. First, we measured the size and amount of CPS in these strains with immunoblotting and enzyme-linked immunosorbent assay (ELISA). Strikingly, cells lacking a functional *cpsC* or *cpsD* accumulated a large amount of low molecular weight (LMW) CPS in the protoplast and cell wall fractions after 1 h of induction (Fig. 2). The total amount of CPS, as determined by ELISA, remained unchanged (*SI Appendix*, Fig. S2). This may be because some of the extremely large CPS molecules in the wild-type cells were not efficiently transferred to the membrane, or they might not even enter the sodium dodecyl sulphate–polyacrylamide gel electrophoresis (SDS-PAGE) gel. Consistent with the results from the laboratory of Janet Yother (17, 18), ligation of CPS to the cell wall PG is apparently size independent and does not require CpsCD (34), as the LMW CPS in Δ*cpsC* and Δ*cpsD* strains was anchored to the PG as efficiently. Furthermore, we demonstrate that the Δ*cpsC* and Δ*cpsD* mutants we constructed were not polar because we could at least partially complement them by ectopic expression of *cpsC* and *cpsD* with a P_{spxB} promoter (*SI Appendix*, Fig. S5 and Table S5). Lastly, we sequenced the genome of strains NUS0267 [Δ*cpsE*//P_{Zn}-*cpsE*], NUS0679 [Δ*cpsC* Δ*cpsE*//P_{Zn}-*cpsE*], and NUS0680 [Δ*cpsD* Δ*cpsE*//P_{Zn}-*cpsE*]. We did not find any mutation in the *cps* locus that could account for the phenotype. Besides the *cps* locus, two other mutations were found. One is in *spd_0670* (an insertion of A at base 248), and the other is a point mutation in

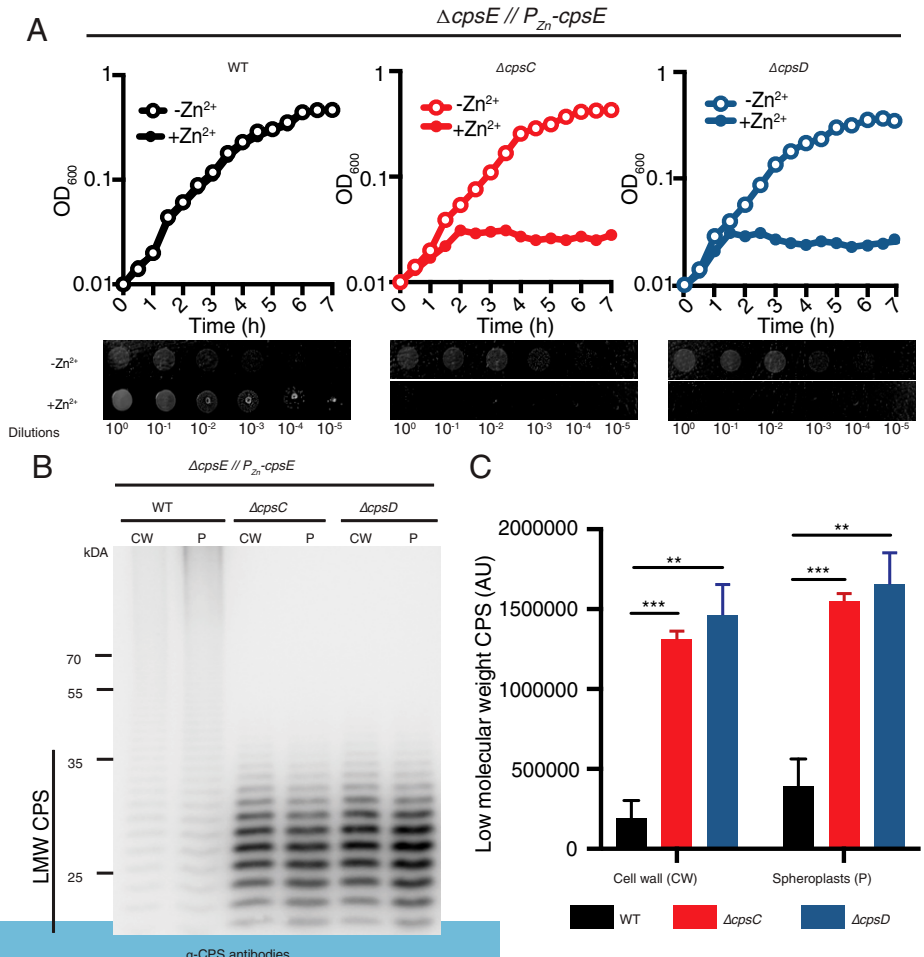

Fig. 2. CpsC and CpsD are required for growth in serotype 2 strain D39. (*A*) Strains NUS0267 [Δ*cpsE*//P_{Zn}-*cpsE*], NUS0679 [Δ*cpsC* Δ*cpsE*//P_{Zn}-*cpsE*], and NUS0680 [Δ*cpsD* Δ*cpsE*//P_{Zn}-*cpsE*] were grown in BHI broth overnight at 37 °C in 5% CO_2. Cultures were diluted in TSB with (solid circles) or without (open circles) Zn^{2+} supplement. Growth was monitored by tracking OD_{600} over time. To test cell viability, cultures of the indicated strains were grown without Zn^{2+} supplement, adjusted to an OD_{600} of 0.2 (10^0 dilution), serial diluted, and spotted on tryptic soy (TS) agar with (*Bottom*) or without (*Top*) Zn^{2+} supplement. Plates were imaged after overnight incubation at 37 °C in 5% CO_2. (*B*) Shown is a representative immunoblot for CPS detection. Cells were grown in TSB until OD_{600} reached 0.2. Cells were harvested and fractionated into cell wall (CW) and protoplast (P) fractions before being separated by SDS-PAGE and transferred to a PVDF membrane. CPS was detected by anti-CPS antibodies. The amount of LMW CPS in each fraction was quantitated by ImageJ (*C*). Means and SDs were calculated from three biological replicates. *P* values were calculated with Student's *t* test. $^{**}P < 0.01$; $^{***}P < 0.001$. Error bars represent the SD.

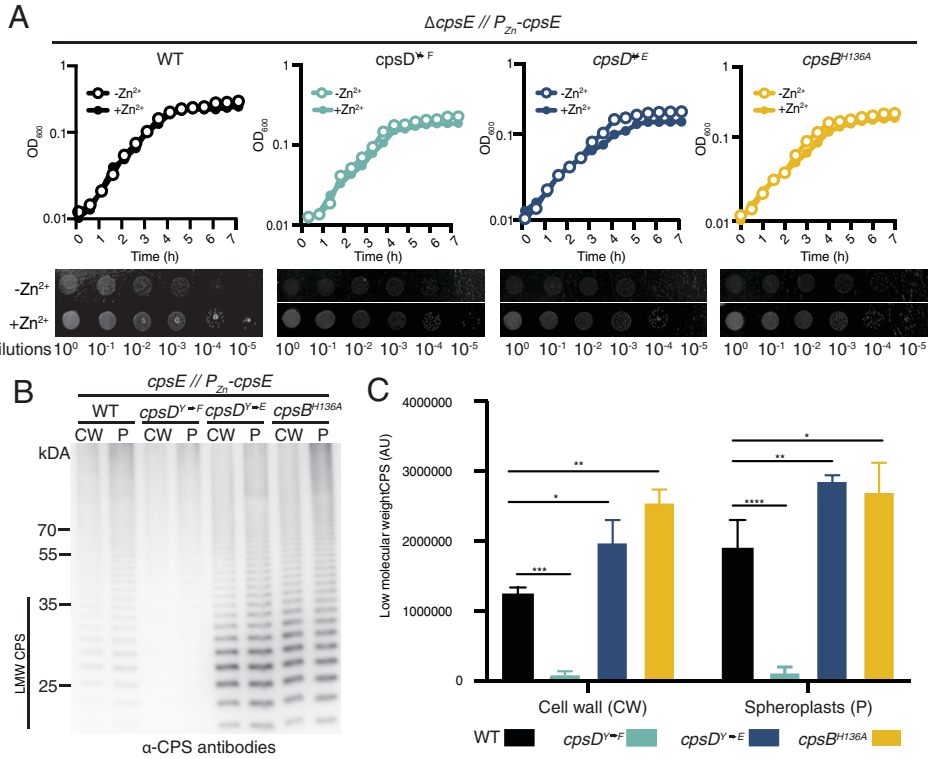

Fig. 3. CpsCD controls the length of the capsule polymers. (*A*) Strains NUS0267 [Δ*cpsE*//P_{Zn}-*cpsE*], NUS0468 [*cpsD*$^{Y\rightarrow F}$ Δ*cpsE*// P_{Zn}-*cpsE*], NUS0469 [*cpsD*$^{Y\rightarrow E}$ Δ*cpsE*//P_{Zn}-*cpsE*], and NUS0430 [*cps2B*^{H136A} Δ*cpsE*// P_{Zn}-*cpsE*] were grown in TSB with or without Zn^{2+} inducer and monitored for growth. To test cell viability, cultures of the indicated strains were adjusted to an OD_{600} of 0.2 (10^0 dilution), serial diluted, and spotted on TS agar with (*Bottom*) or without (*Top*) Zn^{2+} supplement. Plates were imaged after overnight incubation at 37 °C in 5% CO_2. (*B*) Shown is a representative immunoblot for CPS detection. Cells were grown in TSB until the OD_{600} reached 0.2, and Zn^{2+} was added to induce *cpsE* expression. After 1 h, cells were harvested and fractionated into cell wall (CW) and protoplast (P) fractions before being separated by SDS-PAGE and transferred to a PVDF membrane. CPS was detected by anti-CPS antibodies. The amount of LMW CPS in each fraction was quantitated by ImageJ (*C*). Means and SDs were calculated from three biological replicates. *P* values were calculated with Student's *t* test. $*P < 0.05$; $**P < 0.01$; $***P < 0.001$; $****P < 0.0001$. Error bars represent the SD.

spd_1706 (residue 115 E → A). While they are genes of unknown function, they are not likely involved in CPS synthesis because these mutations are also found in the parent strain NUS0267, and this strain produced a normal capsule (*SI Appendix*, Figs. S1 and S2). Together, we conclude that *cpsC* and *cpsD* are essential in serotype 2 strain D39 and required for the production of long CPS polymers.

Mutants that Change the Phosphorylation Status of CpsD Are Viable but with Defective CPS Production. To investigate why CpsC and CpsD are essential, we examined the phosphorylation status of the tyrosine kinase CpsD. We attempted to construct a Δ*cpsD* mutant, but mutations in *cpsE* were simultaneously detected in the transformants recovered (*SI Appendix*, Table S5) (21). Thus, allelic exchange mutants were constructed in the Δ*cpsE*//P_{Zn}-*cpsE* background to prevent the accumulation of undesirable suppressor mutations. The C-terminal tyrosine residues of CpsD were changed to phospho-mimicking glutamate (*cpsD*$^{Y\rightarrow E}$) or nonphosphorylable phenylalanine (*cpsD*$^{Y\rightarrow F}$) residues. In addition, a Δ*cpsB* mutant and an active-site mutant of CpsB phosphatase activity (*cpsB*^{H136A}) (29) were constructed to investigate the role of *cpsB* phosphatase activity on growth and CPS production. We measured the level of phosphorylated CpsD (CpsD~P) by immunoblotting using anti-phosphotyrosine antibodies. As predicted, cells harboring the Δ*cpsB* and *cpsB*^{H136A} mutations had a significant increase in the steady-state level of CpsD~P (*SI Appendix*, Fig. S6). Unsurprisingly, no CpsD~P was detected in the Δ*cpsC*, Δ*cpsD*, *cpsD*$^{Y\rightarrow F}$, and *cpsD*$^{Y\rightarrow E}$ mutants (*SI Appendix*, Fig. S6). None of these mutations were lethal regardless of *cpsE* expression (Fig. 3 and *SI Appendix*, Fig. S7 and Table S6), suggesting the autokinase activity of CpsD is not required for growth. We then quantified the amount of CPS in these strains by immunoblotting. Cells harboring *cpsD*$^{Y\rightarrow F}$ synthesized very little LMW CPS (Fig. 3). In contrast, cells expressing *cpsD*$^{Y\rightarrow E}$, *cpsB*^{H136A}, or with *cpsB* deleted produced significantly more LMW CPS (Fig. 3 and *SI Appendix*, Fig. S7). These results indicate that CpsD phosphorylation leads to a mild accumulation of shorter polymers. CPS production in *S. pneumoniae* does not seem to require cycling between CpsD and CpsD~P because the phosphomimicry *cpsD* and *cpsB* phosphatase mutants both produced an indistinguishable amount of CPS compared to the wild-type cell (*SI Appendix*, Fig. S2). In addition, our results do not support the proposal that CpsD phosphorylation is involved in conjugating CPS to the PG (34) because the relative distribution of CPS in the PG and spheroplasts fractions remained unchanged in all the *cpsC* and *cpsD* mutants we tested.

CpsC Extracellular Loop Is Important for Production for Long Polymers and Cell Viability. Given that the phosphorylation status of CpsD affects the length of CPS polymers, we hypothesized that CpsC and CpsD may interact with the CPS polymerase CpsH, and their interactions may be dependent on CpsD phosphorylation. To test this, we performed a bacterial two-hybrid assay (BACTH). CpsC and CpsH self-interacted. In addition, CpsH interacted with CpsC, but we did not detect interaction between CpsD and CpsH (Fig. 4). The phosphorylation status of CpsD did not affect its interaction with CpsC because mutating the tyrosine residues in CpsD did not alter CpsC and CpsD interaction. To validate the BACTH results, we conducted immunoprecipitation experiments in *S. pneumoniae*. First, we fused CpsC and CpsD with a C-terminal tandem FLAG tag (L-$FLAG_3$) and CpsH with a His_{10} tag at the native loci in order to maintain the expression level. The tagged proteins were functional and stable because they could replace the corresponding wild-type proteins, and no significant degradation was detected by immunoblotting (*SI Appendix*, Fig. S8). When CpsC and CpsD were immunoprecipitated, CpsH readily copurified (Fig. 4). On the contrary, CpsH-his_{10} could not be detected in the eluate fraction if CpsC or CpsD was not FLAG tagged. The coimmunoprecipitation of CpsD and CpsH was probably due to indirect interactions bridged by other CPS proteins. We also noticed that upon immunoprecipitation, CpsH-his_{10} formed an SDS-insoluble aggregate that changed

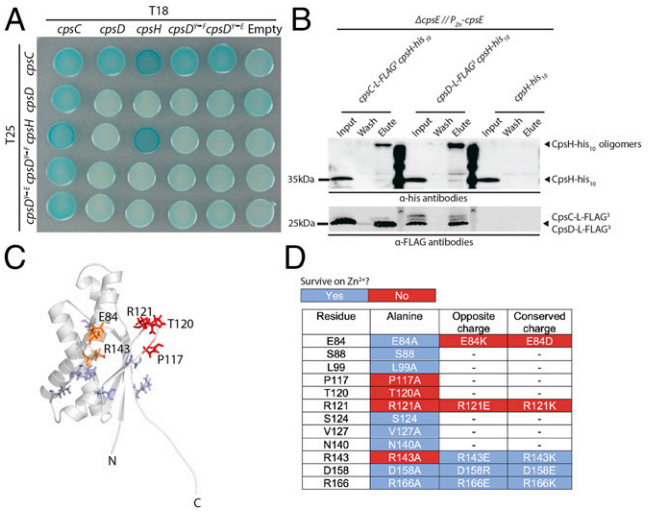

Residue	Alanine	Opposite charge	Conserved charge
E84	E84A	E84K	E84D
S88	S88	-	-
L99	L99A	-	-
P117	P117A	-	-
T120	T120A	-	-
R121	R121A	R121E	R121K
S124	S124	-	-
V127	V127A	-	-
N140	N140A	-	-
R143	R143A	R143E	R143K
D158	D158A	D158R	D158E
R166	R166A	R166E	R166K

Fig. 4. CpsC interacts with CpsD and CpsH and the critical residues of CpsC. (*A*) *E. coli* strain BTH101 harboring plasmids with the indicated genes (*SI Appendix*, Table S8) were grown in LB medium and spotted on LB plates supplemented with 5-bromo-4-chloro-3-indolyl-β-D-galactopyranoside and isopropyl β-D-1-thiogalactoside. Plates were incubated overnight at 37 °C and imaged. (*B*) Coimmunoprecipitation of CpsC, CpsD, and CpsH. Strains NUS1085 [Δ*cpsE cpsH-his*$_{10}$*/*P$_{Zn}$*-cpsE*], NUS1334 [*cpsC*-L-FLAG$_3$ Δ*cpsE cpsH-*$_{his10}$*/*P$_{Zn}$*-cpsE*], and NUS1335 [*cpsD*-L-FLAG$_3$ Δ*cpsE cpsH-*$_{his10}$*/* P$_{Zn}$*-cpsE*] were grown in BHI broth and induced by adding Zn^{2+}. Cells were harvested after 1 h, lysed, and solubilized by adding DDM. The dissolved proteins were immunoprecipitated with anti-FLAG magnetic beads and eluted with 3× FLAG peptide. The eluate fractions were blotted with anti-his tag or anti-FLAG antibodies to detect the bait and prey proteins, respectively. Experiments were done three times with similar results. (*C*) Structure of the extracellular loop of CpsC modeled by I-TASSER. Residues that were mutated were highlighted with colored sticks. Blue: mutable residues; red: immutable residues; orange: partially immutable residues. (*D*) Selected residues of CpsC extracellular loop were mutated to alanine, same charge, or opposite charge residues. Blue: variants that retain CpsC function; red: nonfunctional variants.

its mobility on the SDS-PAGE gel. Despite numerous attempts (see *Materials and Methods*), the CpsH-his$_{10}$ aggregate could not be redissolved. Nevertheless, since the CpsH-his$_{10}$ aggregate was not present in the negative control, we conclude that the CpsCD complex interacts with CpsH in vivo. Similar interactions were reported in other systems (16, 35), and our result is consistent with the observation that the C-terminal region of CpsC (*cpsC*-Δ*Cter*) and CpsD partially recruit CpsH to the septal region (28).

So far, we have demonstrated that the CpsB phosphatase activity and the CpsD autokinase activity are dispensable for growth. Next, we investigated if the disruption of the putative CpsC copolymerase activity is lethal. CpsCD belongs to the polysaccharide copolymerase 2b (PCP2b) family (36). The residues critical for activity are likely located at the CpsC extracellular loop because this domain is structurally similar to the Wzz copolymerase (37). Nevertheless, the exact enzymatic activity of CpsC, as well as the location of the CpsC active site, are still unclear. Thus, we performed a high-throughput mutagenesis coupled with a next-generation sequencing (Mut-seq) experiment (38) to identify the residues required for CpsC function. First, PCR mutagenesis was used to introduce single-nucleotide changes (SNPs) in the *cpsC* allele, and the mutagenized amplicons were transformed into strain NUS0426 [*rpsL1* Δ*cpsE* Δ*cpsC*::P-*sacB-kan-rpsL*$^+$//Δ*bgaA*::P$_{Zn}$-*cpsE*]. Upon selection on medium supplemented with Zn^{2+}, only the cells harboring a functional copy of *cpsC* could survive (Fig. 4). The frequencies of the recovered SNPs were compared with the control without selection, which would indicate the fitness of the individual mutations. Strikingly, the critical residues of CpsC are clustered on the same side of the extracellular loop (Fig. 4 and *SI Appendix*, Fig. S9). This side is supposedly within the chamber formed by the CpsC oligomers and was proposed to interact with the polymerase (39) (Fig. 4). To validate the Mut-seq results, we mutagenized a selection of charged residues at the extracellular loop of CpsC to alanine, same charge residues or opposite charge residues, and examined whether the resulting proteins remained functional (Fig. 4 and *SI Appendix*, Fig. S10). Changes in residues E84, P117, T120, R121, and R143 were not tolerated, suggesting that they are indispensable for CpsC function (*SI Appendix*, Figs. S9 and S10). Unlike the viable CpsC mutants, these nonfunctional variants could no longer support long CPS synthesis (*SI Appendix*, Fig. S10). With the exception of T120, all other nonfunctional CpsC variants retained their ability to interact with CpsD and CpsH, indicating that their inability to activate CpsH was not due to general protein misfolding (*SI Appendix*, Fig. S10). The activity of the CpsCD complex is therefore required for viability, and this activity involves the extracellular loop of CpsC.

CpsC and CpsD Are Required for PG and CPS Coordination. To our knowledge, there is no report of essential PCP protein under laboratory conditions. Why the loss of CpsCD resulted in cell death is intriguing. CpsC has been suggested to coordinate CPS synthesis with the cell cycle (28, 30, 40). The spatiotemporal coordination ensures that both daughter cells are completely covered with CPS, which could be crucial to their survival. To visualize the interplay between PG and CPS synthesis, we first labeled the old PG with the fluorescent D-amino acid (FDAA) BODIPY-FL 3-amino-D-alanine (BADA) (41). After the label was evenly integrated into the cell wall, BADA was washed away, and CPS production was induced by the addition of Zn^{2+}. Simultaneously, we added another FDAA HADA (3-[7-hydroxycoumarin]-carboxamide-D-alanine) to chase the synthesis of the new PG. Cells were harvested at 15-min intervals and heat inactivated followed by immunostaining with anti-CPS antibodies (*SI Appendix*, Fig. S11). Like PG synthesis, CPS synthesis was also initiated at mid-cell and propagated along the long axis of the bacteria (Fig. 5) (42, 43). To visualize the synthesis of CPS in labeled cells at a higher resolution, we performed three-dimensional structural illumination microscopy (3D-SIM). This technique allowed us to clearly observe the sites of CPS synthesis, and we showed that they mostly colocalized with PG synthesis 15 min after induction (Fig. 5 and Video S1). The CPS formed an outer ring that surrounded the cell envelope. Our cell biology data suggest that CPS synthesis and PG synthesis are coordinated to ensure the orderly assembly of the bacterial cell envelope.

Next, we investigated the effect of *cpsC* and *cpsD* deletions on the localization of CPS and PG synthesis. Previous studies showed that CPS was not detected at the division septum of the Δ*cpsC* and Δ*cpsD* mutants (28, 30), suggesting that CpsCD is a spatial regulator organizing the CPS complex. We reasoned that the inability to direct the CPS complex to the septal region may be lethal to the cell, similar to the need to localize PG synthase PBP1a in pneumococcus (44). To test this notion, we used the same pulse–chase experiment described to examine CPS and PG synthesis in the Δ*cpsC* and Δ*cpsD* mutants. Cells were pulsed and chased with BADA and HADA, respectively, while CPS synthesis was induced before immunostaining. We demonstrated that when *cpsC* or *cpsD* was disrupted, part of the CPS was no longer colocalized with the site of new PG synthesis (Fig. 6 and *SI Appendix*, Figs. S11 and S12). FDAA incorporation was at a similar pace at the 15- and 30-min time points. However, 45 and 60 min after *cpsE* induction, significantly less PG synthesis was observed compared to the

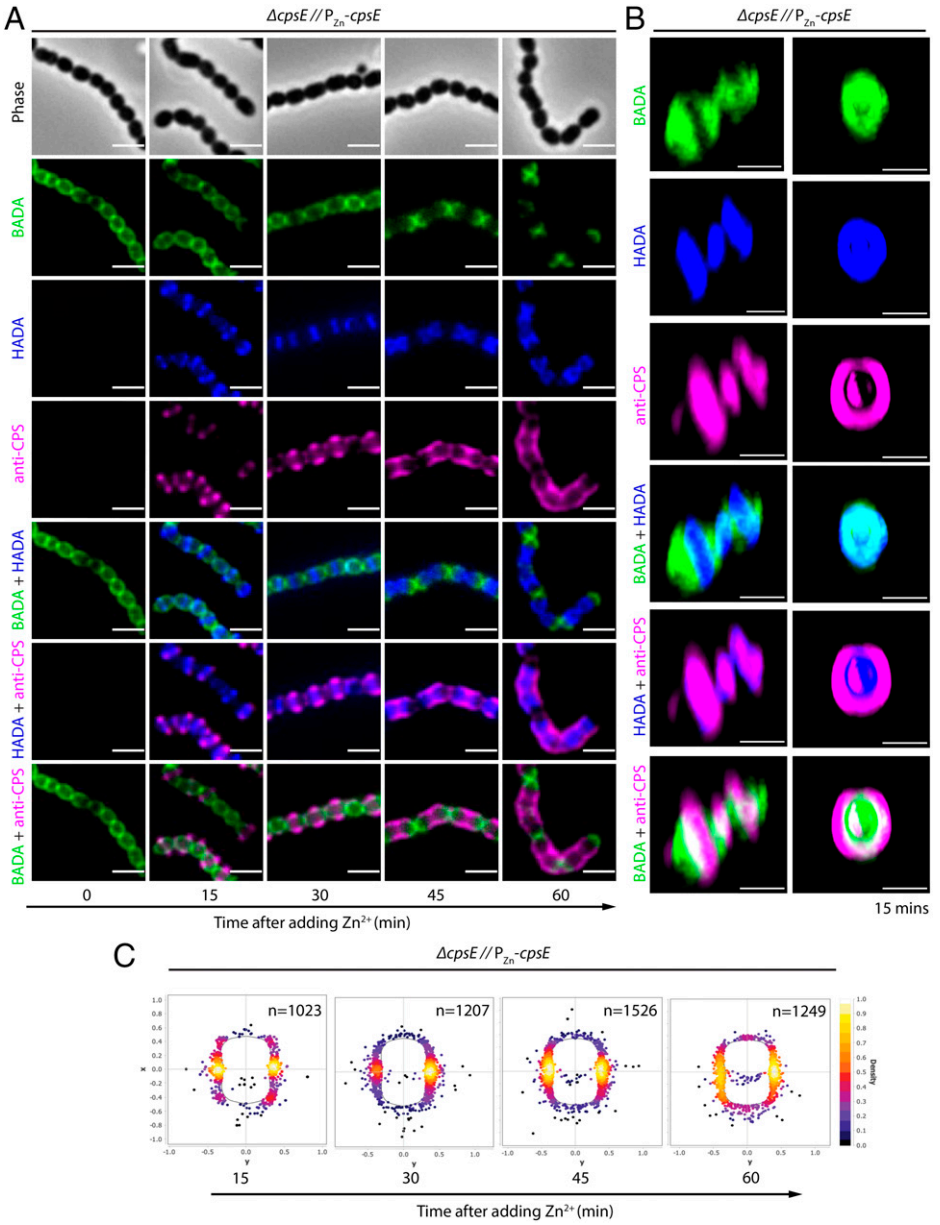

Fig. 5. Coordination between CPS and PG synthesis. (*A*) Strain NUS0267 [Δ*cpsE*//P$_{Zn}$-*cpsE*] was grown and labeled with BADA (old PG) and washed, and CPS production was induced by adding Zn^{2+}. HADA (new PG) was immediately added, and growth was resumed by incubating at 37 °C. Bacteria were harvested every 15 min, heat killed, and stained with anti-serotype 2 CPS antibodies (anti-CPS) and Alexa Fluor 647–labeled goat anti-rabbit secondary antibodies. Labeled cells were imaged by fluorescent microscopy or (*B*) 3D-SIM. Scale bar, 2 μm. For 3D-SIM, the 15-min time point was used as a representative. (*C*) The signal from the anti-CPS channel was analyzed by MicrobeJ.

wild-type cells (Figs. 5 and 6). In ∼100 cells we observed, only 12.2% of the Δ*cpsC* cells and 12.4% of the Δ*cpsD* cells displayed any detectable CPS, and if present, the anti-CPS labels delocalized (Fig. 6 and *SI Appendix*, Fig. S12). In these cells, the intensity of the CPS labels was much weaker, which prevented us from obtaining higher-resolution images through SIM. However, caution should be taken when interpreting this result, as the weaker signal may be due to delocalization of CPS synthesis. Indeed, when we measured the amount of CPS by ELISA, the Δ*cpsC* and Δ*cpsD* cells produced a similar amount of CPS (*SI Appendix*, Fig. S2). The inability to recruit the CPS synthesis machinery to the septal region is not the cause of cell death, as cells expressing a nonfunctional variant of *cpsC* retained CPS synthesis at the septum after *cpsE* induction, although the synthesis did not propagate along the long axis of the cell, and they eventually died (*SI Appendix*, Fig. S13). Lastly, the changes in the CPS-labeling pattern were unlikely due to an overall change in shape of the Δ*cpsC* or Δ*cpsD* mutants because cells were harvested prior to the onset of cell shape defects (Fig. 6 and *SI Appendix*, Fig. S12).

Δ*cpsC* and Δ*cpsD* Mutants Have Reduced Und-P Levels. The inhibition of PG synthesis in the Δ*cpsC* and Δ*cpsD* mutants suggested a shortage of PG precursor(s). This may be due to Und-P sequestration (21). To test this, we examined whether the Δ*cpsC* and Δ*cpsD* mutants were hypersensitive to bacitracin. Bacitracin reduces the availability of Und-P by directly binding to undecaprenyl pyrophosphate (Und-PP) (45) (Fig. 1*B*). If *cpsC* and *cpsD* deletions indeed sequester Und-P, the minimal inhibitory concentrations (MICs) of bacitracin would be significantly reduced. We determined the sublethal dose of Zn^{2+} that allowed the growth of *cpsC* and *cpsD* mutants to be 100 μM (*SI Appendix*, Fig. S14). Similarly, the MIC of bacitracin is 125 ng/mL for the wild-type cells. We employed the Δ*cpsH* mutant as a positive control because the lack of CPS polymerase activity was postulated to sequester Und-P (21). As expected, wild-type cells grew normally at sublethal concentrations of Zn^{2+} and bacitracin. In contrast, the Δ*cpsC*, Δ*cpsD*, and Δ*cpsH* mutants were more sensitive to bacitracin (Fig. 7*A*) in which both Δ*cpsC* and Δ*cpsD* mutant had reduced MICs (62.5 ng/mL). This suggests that the cell may have fewer free

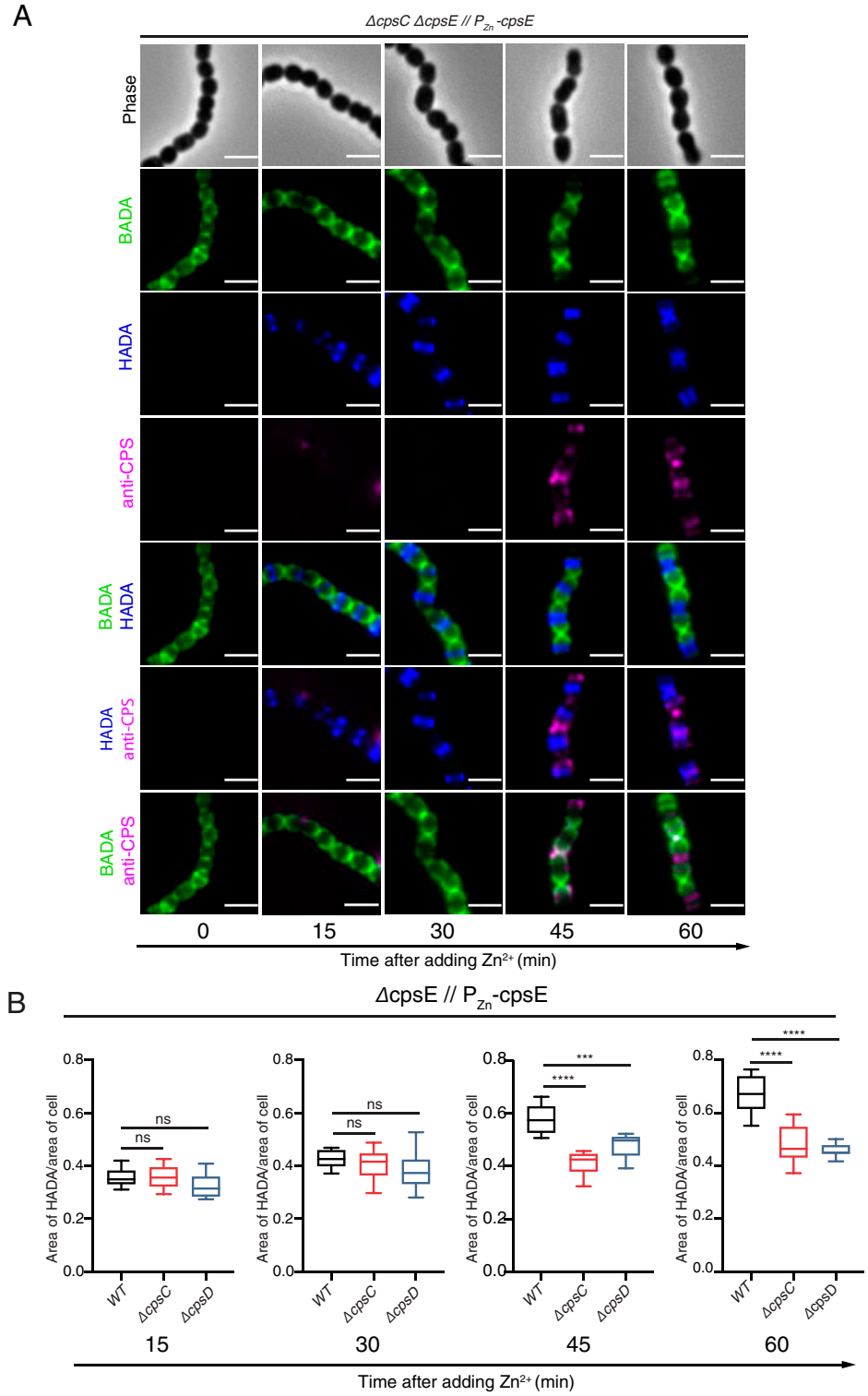

Fig. 6. Inactivation of CpsC disrupts the assembly of CPS and PG. (*A*) Strain NUS0679 [Δ*cpsC* Δ*cpsE*//P$_{Zn}$-*cpsE*] was grown, induced, labeled with BADA (old PG) then HADA (new PG), heat inactivated, and immunostained as described in the legend of Fig. 5. Scale bar, 2 μm. (*B*) Incorporation of new PG at different time points (n = 20). Images of the wild-type and the Δ*cpsD* strains are shown in Fig. 5*A* and *SI Appendix*, Fig. S12, respectively. P values were calculated with Student's t test. ***P < 0.001; ****P < 0.0001; ns, not significant. Error bars represent the SD.

Und-P molecules. To exclude the possibility that both the Δ*cpsC* and Δ*cpsD* mutant in general have an increased sensitivity to cell wall–acting antibiotics, we tested the mutants with another cell wall–targeting antibiotic: methicillin. Methicillin is a β-lactam antibiotic that blocks PG synthesis by inhibiting the transpeptidase activity of penicillin-binding proteins (PBPs), mainly PBP2x (46, 47). We demonstrate that the MIC of methicillin (0.25 μg/mL) remains unchanged in Δ*cpsC* and Δ*cpsD* cells as compared to the wild-type cells (*SI Appendix*, Fig. S15). The increased sensitivity to bacitracin could be corrected by complementing *cpsC* and *cpsD* in *trans* (*SI Appendix*, Fig. S16). Consistent with this result, mass spectrometry revealed the cellular amount of Und-P was significantly lower in the Δ*cpsD* and Δ*cpsH* mutants (Fig. 7 and *SI Appendix*, Fig. S17). Together, our data suggests that inhibition of PG synthesis in *cpsC* and *cpsD* mutants was likely caused by Und-P

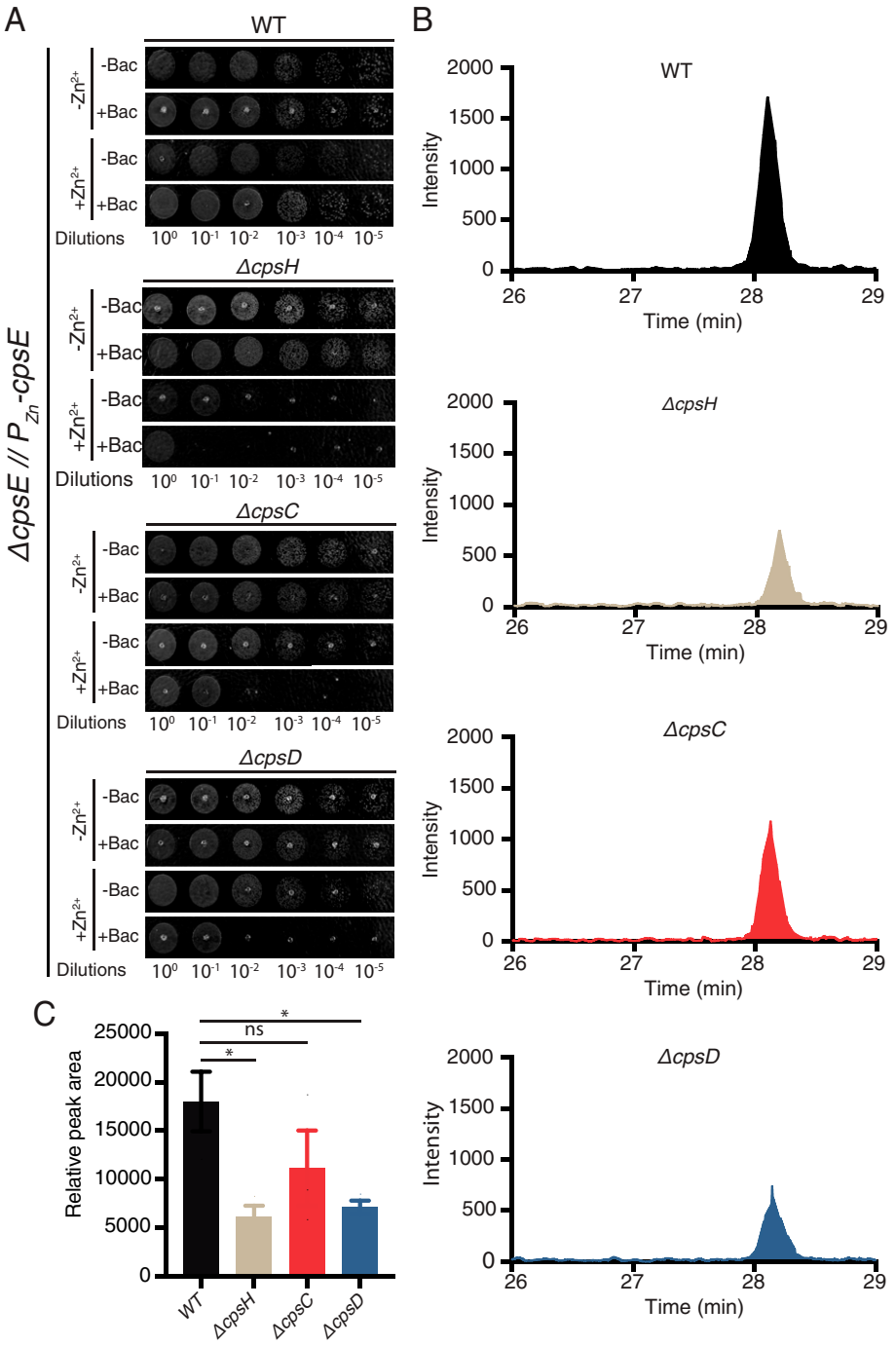

Fig. 7. Inactivation of CpsC, CpsD, and CpsH sequesters Und-P. (*A*) Strains NUS0267 [Δ*cpsE*//P_{Zn}- *cpsE*], NUS0679 [Δ*cpsC* Δ*cpsE*//P_{Zn} -*cpsE*], NUS0680 [Δ*cpsD* Δ*cpsE*//P_{Zn} -*cpsE*], and NUS0732 [Δ*cpsH* Δ*cpsE*//P_{Zn} -*cpsE*] were grown in BHI broth, serial diluted, and spotted on TS agar supplemented with 0.1 mM $ZnCl_2$,10 μM $MnCl_2$, and 125 ng/mL bacitracin when indicated. Plates were incubated overnight at 37 °C and photographed. (*B*) The same set of strains were grown and induced, and the cells were collected by centrifugation. Lipid was extracted and analyzed by liquid chromatography–mass spectrometry. Shown are representative extracted ion count curves of Und-P (around 28 min; exact masses are provided in *SI Appendix*, Fig. S17), and the quantitation is plotted in *C*. Means and SDs were calculated from three biological replicates. *P* values were calculated with Student's *t* test. **P* < 0.05; ns, not significant. Error bars represent the SD.

sequestration, which could be due to premature termination of CPS synthesis.

Discussion

How autophosphorylation affects the activity of BY-kinase is not fully understood. In this paper, we present evidence that the BY-kinase CpsCD is required for growth in *S. pneumoniae*. Our working model is that the lack of CpsCD disrupts the coordination between CPS and PG synthesis as well as sequesters Und-P (*SI Appendix*, Fig. S18). The sequestration is likely due to the accumulation of short Und-linked CPS precursors. While these intermediates can be further polymerized into full-length CPS, they deplete the scarce Und-P lipid carrier needed for cell envelope synthesis, which subsequently kills the cell (*SI Appendix*, Fig. S18).

We also showed that CpsD autophosphorylation modulates the length of the CPS. The change in size of the CPS polymers was not due to altered interactions between CpsC, CpsD, and CpsH upon CpsD phosphorylation. Structural studies of CapB suggested BY-kinase autophosphorylation releases the constraints of the transmembrane domain of the oligomeric ring and activates the kinase activity (48). It is tempting to speculate that this change will also transduce a signal that activates the CpsC periplasmic domain. Our Mut-seq analysis supports this model because the key residues required for CpsC function are

all pointing toward the lumen of the oligomeric rings in the CpsC structural model (Fig. 4). As the CpsC extracellular loop is similar to the Wzz copolymerase, CpsC may modulate CpsH activity or processivity in response to a change in the phosphorylation state of CpsD. Nevertheless, our results did not exclude other possible enzymatic functions of CpsC, such as cleaving lipid-linked precursors (31), ligating CPS to PG (34), and transporting CPS precursors across the cytoplasmic membrane (30). Ongoing work is underway to reconstitute the CpsCD system for further investigation into the activation mechanism and enzymatic activity.

The significance of regulating the length of bacterial glycans has been reviewed recently (36). In brief, controlling the distribution of glycan length assists pathogens to survive in various host niches. This has been demonstrated in the *Salmonella* LPS pathway (49, 50) in which a minimum of four to five repeating units are required to confer serum resistance, whereas the "very long" LPS polymers favor survival if the cells are exposed to bile salts and antimicrobial peptides at the intestinal epithelia. Probably the surface glycans serve as a decoy when shredded (51–53). We found that as the cell synthesizes longer polymers, the number of glycan molecules on the cell surface decreases (Fig. 3 and *SI Appendix*, Fig. S2). Thus, due to the limited reservoir of sugars and Und-P, it is crucial for the cell to strike a balance between the glycan length and abundance. We propose that CpsBCD controls the length of CPS polymers through CpsD phosphorylation in response to external stimuli. It was shown that in the low O_2 environment, CpsB phosphatase activity is reduced with a concomitant increase in the CpsD~P level (29). Shorter but more molecules of CPS polymers will be produced. The extra CPS molecules can cover vulnerable regions such as the division septum, where the capsule is thinner (54). In contrast, lesser CpsD~P is accumulated in the high O_2 condition. This may result in the formation of "very long" CPS polymers. These polymers may serve the same purpose as the "very long" LPS in *Salmonella*. Notably, producing longer glycan polymers does not necessarily correlate with fitness inside the host. Quite the contrary, the very high molecular weight CPS in the bloodstream may be counterproductive because these glycans may induce more efficacious anti-CPS antibodies with a higher affinity for the capsule layer (55). Further studies will investigate the effect of CPS length on virulence in different host niches.

Materials and Methods

Bacterial Strains and Growth Conditions. Strains used in this study are listed in *SI Appendix*, Table S7. *S. pneumoniae* cells were grown in TSB (BD, 211768) or BHI broth (Thermo Fisher, CM1135B) at 37 °C supplemented in 5% CO_2. Antibiotics were purchased from Sigma-Aldrich and added to a final concentration of 0.3 μg/mL for erythromycin (Erm), 250 μg/mL for kanamycin (Kan), 150 μg/mL for spectinomycin (Spec), and 300 μg/mL for streptomycin (Str). Unless otherwise specified, $ZnCl_2$ and $MnCl_2$ were added to the medium at a final concentration of 0.5 mM and 50 μM, respectively. *Escherichia coli* cells were grown with shaking at temperatures at 30 or 37 °C with aeration in lysogeny broth (LB) (BD, 244620) containing appropriate antibiotics. Kan and ampicillin (Amp) were used at a final concentration of 50 and 100 μg/mL, respectively. Plasmids were maintained in DH5α(λpir) and purified using the Qiagen Miniprep Kit (*SI Appendix*, Table S8) before transforming into the corresponding *E. coli* strains.

S. pneumoniae strains were constructed by transforming PCR amplicons or isothermal assembly products after inducing natural competence (56). Briefly, PCR fragments were prepared using Phusion High-Fidelity DNA Polymerase (NEB, M0530S), diagnosed by gel electrophoresis, and purified using the QIAquick PCR Purification Kit (Qiagen, 28106). Allelic exchange was done by positive and negative selection using the Sweet Janus (57), the Janus (58), or an erythromycin-resistant derivative of the Janus cassettes. Transformants were plated and streaked on tryptic soy agar (TSA)-II plates supplemented with 5% defibrillated sheep blood (BD, 221261) and appropriate antibiotics. The presence and integrity of genetic constructs were confirmed by diagnostic PCR using the GoTaq polymerase (Promega, M712) and Sanger sequencing. Oligonucleotides for synthesizing PCR amplicons are listed in *SI Appendix*, Table S9.

For growth curves, overnight cultures of the indicated strains were diluted in BHI broth or TSB to a starting optical density at 600 nm (OD_{600}) of 0.01. Optical densities were measured using the GeneSys 30 spectrophotometer (Thermo). The diluted cultures were grown at 37 °C in 5% CO_2, and the OD_{600} readings were measured every 30 min. When appropriate, cultures at OD_{600} of 0.15 to 0.2 were serial diluted and spotted on BHI agar or TS agar supplemented with 0.1 mg/mL catalase. For bacitracin and methicillin sensitivity assay, where indicated, the TS agar plates were supplemented with 0.1 mM $ZnCl_2$,10 μM $MnCl_2$, and 125 ng/mL bacitracin (Precision Technology, S4146).

Tn-Seq. Tn-seq was performed essentially as described before (44). In vitro transposition was done by mixing 10 μl buffer A (38.7 mM Hepes pH 7.9, 178 mM NaCl, 35.5 mM $MgCl_2$, 19% [vol/vol] glycerol, 3.8 mM 1,4 dithiothreitol [DTT], and 1.9 mg/mL bovine serum albumin [BSA]), 1 μg genomic DNA prepared from strain D39, 1 μg pMagellan6 plasmid, and 1.4 μg purified MarC9 transposase. The mixture was incubated overnight at 30 °C and purified using the Qiagen DNeasy Blood and Tissue Kit (Qiagen, 69504). Transposed DNA was diluted in water to a final volume of 49 μl, and then 6.6 μl buffer B (0.5 M Tris HCl pH 7.83, 100 mM MgCl2, and 10 mM DTT), 6.6 μl 10 mg/mL BSA, 2.5 μl 2 mM dNTPs, and 2.5 μl T4 DNA polymerase (NEB, M0203L) were added to the DNA and incubated for 30 min at room temperature. After incubation, 2.5 μl 2.6 mM NAD^+, 2.5 μl *E. coli* DNA ligase (NEB, M0205L), and 0.5 μl 10 mg/mL BSA were added to the mixture and further incubated at room temperature overnight. The repaired DNA was transformed into strain IU1781 (D39 *rpsL1*) or HMS0002 (D39 *rpsL1* Δ*cpsE*). The sizes of the wild-type and Δ*cpsE* libraries were estimated to be 90,000 and 60,000 transformants, respectively. Colonies were dislodged by scraping the plates and then were resuspended in 2 mL BHI medium and pooled, and genomic DNA was extracted using the MasterPure DNA Extraction Kit (Scientific Resources, MGP04100). Purified DNA was digested by MmeI (NEB, R0637S), treated with calf intestinal alkaline phosphatase (NEB, M0290S), and ligated to the next-generation sequencing adaptors (59). The ligation products were amplified by the KAPA Library Amplification Kit (Roche, KK2611) with primers P1_Miseq_MmeI and GEX_P2, gel purified, and sequenced on an Illumina MiSeq platform. Data analysis was done exactly as previously described in Fenton et al. (44) and Flores-Kim et al. (60) using CLC Genomics Workbench (Qiagen) and custom-made Python and R scripts (44). Briefly, reads were normalized to the library with the lower number of reads. They are demultiplexed, trimmed, and aligned to the D39 genome. Statistical analysis was performed using a Mann–Whitney *U* test to identify genomic regions with significant differences in transposon insertion profiles. Selected hits are presented in *SI Appendix*, Table S2, and additional information is provided in Dataset S2.

Immunoblotting. The quantity and size of CPS were measured by immunoblotting as described in Geno et al. with minor modifications (21). Cells of the indicated strains were grown in TSB to an OD_{600} of 0.2 before induction by adding $ZnCl_2$ and $MnCl_2$. Cultures were incubated for 1 h at 37 °C in 5% CO_2, normalized to OD_{600} of 0.2, and 1 mL culture was centrifuged at 16,100 x *g* for 1 min at room temperature. The spent medium was discarded, and the cell pellets were washed once with phosphate-buffered saline (PBS; 137 mM NaCl, 2.7 mM KCl, 1 mM $CaCl_2$, 0.5 mM $MgCl_2$, 10 mM Na_2HPO_4, and 1.8 mM KH_2PO_4, pH 7.4). For fractionation, samples were resuspended in 200 μl protoplast buffer (50 mM Tris HCl pH 7, 50 mM $MgCl_2$, and 20% [wt/vol] sucrose). Protoplasts were prepared by adding 40 units of mutanolysin (Sigma, M9901) and 25 μg lysozyme (Axil Scientific, L-040-25) and incubated overnight at room temperature. The digestion was evaluated by the formation of round spheroplasts. The protoplasts were collected by centrifugation at 3,000 × *g* for 10 min at room temperature. The supernatant fractions were collected (i.e., cell wall fraction), and the protoplasts were lysed by resuspending in an equal volume of PBS. For whole-cell pellets samples, samples were resuspended in 200 μl PBS. The samples were mixed with an equal volume of 2× Laemmli buffer, and 2 μl proteinase K (Qiagen, 19133) was added to digest the cellular protein at 56 °C for 1 h. CPS was resolved on a 10% SDS-PAGE gel or a 16% (wt/vol) Tris-Tricine gel, transferred to a polyvinylidene fluoride (PVDF) membrane, and blocked for 30 min at room temperature in blocking buffer (PBS with 0.05% [vol/vol] Tween 20 and 5% [wt/vol] skimmed milk). Blots were probed with anti-serotype 2 CPS antiserum (SSI Diagnostica) at a 1:5,000 dilution at 4 °C overnight in blocking buffer, washed twice with PBST (PBS with 0.05% [vol/vol] Tween 20), and detected by goat anti-rabbit horseradish peroxidase (HRP) antibodies (Thermo Fisher, A16110) at a 1:10,000 dilution. The membranes were washed three times with PBST and developed with a chemiluminescent substrate (Thermo Fisher, 34580).

CpsD~P was quantified essentially as described by Bender and Yother (17). Briefly, cells were grown in BHI broth to an OD_{600} of 0.2. Cultures were induced by adding $ZnCl_2$ and $MnCl_2$ and incubated for 1 h at 37 °C in 5% CO_2. Cells were normalized to an OD_{600} of 0.2 and collected by centrifugation at 16,100 × *g* for 5 min at room temperature. Pellets were washed once with 1 mL PBS and resuspended in 40 μl PBS. An equal volume of 2× Laemmli buffer was added followed by the addition of 0.5 μl protease inhibitor mixture (Merck, 539134–1MLCN). The samples were boiled for 10 min and centrifuged at 16,100 × *g* for 1 min at room temperature to remove cell debris. The supernatant fractions were collected and resolved on a 15% SDS-PAGE gel, transferred to a PVDF membrane, and incubated in blocking buffer for 30 min at room temperature. The membrane was blotted with anti-phosphotyrosine antibodies (Santa Cruz Biotechnology, sc-7020) at a 1:1,000 dilution and goat anti-mouse HRP (Thermo Fisher, A16110) at a 1:10,000 dilution and developed with a chemiluminescent substrate.

ELISA. Cross-adsorbed anti-serotype 2 CPS antiserum was prepared as described in ref. 21. Briefly, cells of an unencapsulated strain (D39 *rpsL1* Δ*cpsE*) were grown in 50 mL BHI broth until the OD_{600} reading was between 0.6 and 0.8. Cells were washed once with 1 mL PBS and inactivated by incubating at 65 °C for 45 min. Heat-killed cells were resuspended in PBS at a final OD_{600} of 0.9. For cross-adsorption, 8 μl anti-serotype 2 CPS antiserum was mixed with 280 μl heat-killed cells and 8 mL PBS with 1% (wt/vol) BSA. The mixture was incubated overnight at 4 °C, and the heat-killed cells were removed by centrifugation and filtration through a 0.22-μm filter (Costar, CLS8160). The adsorbed antiserum was stored at 4 °C until use.

Cells of the indicated strains were grown in 40 mL TSB. When the culture reached an OD_{600} of 0.2, cells were induced by adding $ZnCl_2$ and $MnCl_2$. After 1 h of induction, culture densities were normalized to an OD_{600} of 0.4, and the cells were harvested by centrifugation at 16,100 × *g* for 1 min at room temperature. Pellets were resuspended in an equal volume of PBS. Samples in a 100-μl volume were treated by adding 2.5 μl proteinase K (Qiagen, 19133) and incubated at 56 °C for 1 h. Supernatant was removed by centrifugation, and pellets were resuspended in 50 mM carbonate/bicarbonate buffer (Sigma, C3041). The suspension was added to ELISA plates (Thermo Fisher, 442404) and incubated overnight at 4 °C. Serial-diluted serotype 2 CPS (SSI Diagnostica) dissolved in carbonate/bicarbonate buffer was used as an internal standard. ELISA plates were washed with PBS and blocked by incubating in PBS with 1% (wt/vol) BSA for 1 h at room temperature. Wells were washed four times with PBST, and cross-adsorbed anti-serotype 2 CPS antiserum (SSI Diagnostica) was added at a 1:1,000 dilution followed by incubation for 1 h at room temperature. Plates were washed four times with PBST, and goat anti-rabbit HRP antibodies (Thermo Fisher, A16110) were added at a 1:1,000 dilution in 1× PBS with 1% (wt/vol) BSA. After washing four times with PBST, antibodies were detected by a colorimetric OPD (*o*-phenylenediamine dihydrochloride) substrate (Sigma, P9187-50SET) according to the manufacturer's protocol. Optical density at 450 nm (OD_{450}) was recorded with a Tecan plate reader, and the CPS was quantitated by extrapolating the OD_{450} values of the samples and the purified CPS standards.

To measure the CPS released to the medium, cells of the indicated strains were grown in BHI overnight at 37 °C in 5% CO_2. Cultures were diluted to an OD_{600} of 0.01 and continued to grow until the optical density reached 0.1. To induce *cpsE* expression, Zn^{2+} and Mn^{2+} were added to a final concentration of 0.5 and 0.05 mM, respectively. After 1 h, cultures were normalized to an OD_{600} of 0.2, and 1-mL fractions were collected. For one fraction, spent medium was collected by centrifugation at 16,000 × *g* for 1 min at room temperature. Another fraction was used directly to measure the total amount of CPS in the culture. An equal volume of the spent medium and culture was mixed separately with 50 μl 0.2 M of sodium carbonate-bicarbonate buffer (Sigma, C3041). Cellular protein was digested by adding 4 μl proteinase K (Qiagen, 19133) and incubated at 37 °C for 2 h. After digestion, 100 μl samples were serial diluted, adjusted to a final volume of 50 μl, and transferred to an ELISA plate. The plates were incubated at 4 °C overnight, blocked with 1% (wt/vol) BSA for 1 h at room temperature, and detected with cross-adsorpted anti-serotype 2 CPS antisera at a 1:1,000 dilution for 1 h at room temperature. The wells were washed with PBST four times between each incubation step and finally detected with anti-rabbit HRP antibodies in 1% (wt/vol) BSA at a 1:1,000 dilution for 1 h. After washing, plates were developed by adding the OPD substrate, and OD_{450} was measured with a plate reader.

BACTH Experiments. BACTH experiments were performed based on ref. 61 and the manufacturer's instructions (Euromedex). PCR amplicons were synthesized with the Phusion DNA polymerase, genomic DNA of strain D39, and the primers listed in *SI Appendix*, Table S9. PCR products were purified, digested with BamHI and XbaI, and ligated to pKT25 and pCH364 digested with the same enzymes. With this procedure, the indicated open reading frames will be fused to a T25 or T18 adenylate cyclase fragment at the N terminus. Purified plasmids were cotransformed into *E. coli* strain BTH101 by electroporation and plated on LB agar containing 100 μg/mL Amp and 50 μg/mL Kan and incubated overnight at 32 °C. Individual colonies were picked and inoculated in LB broth supplemented with 100 μg/mL Amp and 50 μg/mL Kan and spotted on the plates with the same antibiotics but with 40 μg/mL 5-bromo-4-chloro-3-indolyl-β-D-galactopyranoside and 0.5 mM isopropyl β-D-1-thiogalactoside. The plates were incubated overnight at 32 °C and imaged.

Co-Immunoprecipitation. Immunoprecipitation of FLAG-tagged proteins was done as described elsewhere with slight modifications (61). Cells of the appropriate strains were grown in 40 mL BHI and induced by adding Zn^{2+}. Cultures were normalized to an OD_{600} of 0.2, and the cells were harvested by centrifugation at 16,100 × *g* for 5 min at room temperature. Pellets were washed once with 20 mL PBS and resuspended in cold lysis buffer (50 mM Tris HCl pH 7.4, 150 mM NaCl, and 1 mM ethylenediamine tetraacetic acid [EDTA]) to a final volume of 1 mL The suspension was transferred into two lysing matrix B tubes (MP Biomedicals, 116911050) containing 25 μl EDTA-Free Protease Inhibitor Mixture III (Calbiochem). Bead beating was done with a Precellys Evolution homogenizer (Bertin Instruments) at 6.0 M/s for 40 s, 10 times. Tubes were incubated on ice for 5 min every three or four times of homogenizing to avoid heating. Cell debris and the lysing matrix were removed by centrifugation at 16,100 × *g* for 1 min, and n-dodecyl-B-D-maltoside (DDM) (Anatrace D310) was added to the sample to a final concentration of 1% (wt/vol). Protein concentrations were measured by Bradford assays (Bio-Rad, 5000205) and normalized. Solubilized membrane proteins in a 500-μl volume were mixed with 50 μl anti-FLAG magnetic beads (Sigma, M8823) and incubated for 2 h at 4 °C with shaking. After separation with a magnetic stand, the liquid was discarded, and the beads were washed three times with 1 mL ice-cold lysis buffer with 0.05% (wt/vol) DDM and eluted by incubation for 30 min at 4 °C in 40 μl lysis buffer with 0.05% (wt/vol) DDM and 150 ng 3× FLAG peptide (Sigma, F4799). An equal volume of 2× Laemmli buffer was added to the samples and incubated for 1 h at room temperature. Proteins were separated on a 15% SDS-PAGE gel, transferred onto PVDF membrane, and blocked for 30 min in blocking buffer. His-tagged and FLAG-tagged proteins were detected by blotting with Anti-6x His tag Monoclonal Antibody (Thermo Fisher, MA121315) and anti-FLAG antibodies (Sigma-Aldrich, F7425) at a 1:2,500 dilution, respectively. The membrane was either blotted with sheep anti-rabbit Dylight800 antibodies (Bio-Rad, STAR36D800GA) or goat anti-mouse HRP antibodies (Thermo Fisher, G21040) at a 1:10,000 dilution. Chemiluminescent detection was done using a high-sensitivity substrate (Thermo Fisher, A38556), and the infrared signal was imaged by a Bio-Rad Gel Doc. We noticed that after immunoprecipitation, CpsH-his_{10} formed a high molecular weight aggregate that was not resolved well on an SDS-PAGE gel. Possibly during the washing step, some interacting partner(s) that stabilize CpsH-his_{10} was removed, which led to protein aggregation (62). In attempts to disperse CpsH-his_{10}, different concentrations of DDM (0.05, 0.5, and 1%) were added after homogenization. We also changed the incubation temperature after 2× Laemmli buffer was added. Lastly, we tested if adding 6.0 M urea would denature CpsH-his_{10} and disrupt the aggregation. Unfortunately, none of these attempts, alone or in combination, were able to dissociate the CpsH-his_{10} aggregate.

Mut-Seq. Mut-seq was done as described in refs. 38, 63, and 64 with slight modifications. *cpsC* was PCR mutagenized using the GoTaq DNA polymerase and primers P91 and P552 (*SI Appendix*, Table S9). PCR products were purified and concentrated and transformed into strain NUS0426 [*rpsL1* Δ*cpsE* Δ*cpsC*::P-*sacB-kan-rpsL*$^+$//Δ*bgaA*::P_{Zn}-*cpsE*]. Streptomycin- and sucrose-resistant transformants were pooled and plated on TSA plates with or without Zn^{2+} supplement. Survivors were pooled and suspended in BHI medium and adjusted to an OD_{600} of ~0.7 in BHI medium followed by genomic DNA extraction with the Qiagen DNeasy Blood and Tissue Kit. Next, the *cpsC* region was amplified with primers P91 and P552. PCR amplicons were quantified by the Qubit dsDNA HS Assay Kit (Invitrogen) and sequenced on a NovaSeq platform (GeneWiz). Data analysis was performed using the CLC workbench (Qiagen) software as described in refs. 38, 63, and 64. Briefly, reads were mapped to the *cpsC* region with the length and similarity fraction parameters set to 1. Unmapped reads were collected and aligned with the *cpsC* open reading frame with the similarity fraction reduced to 0.98. Base changes were detected by the variant detection tool of the CLC workbench, consolidated, and exported to Microsoft Excel.

FDAA Pulse–Chase Experiment and Immunofluorescence Microscopy. Cells of the indicated strains were cultured to an OD_{600} of 0.1 to 0.3 and diluted to an OD_{600} of 0.02 in TSB supplemented with 50 mM BADA. After incubation for

2.5 h at 37 °C in 5% CO_2, cells were harvested by centrifugation at 10,000 × *g* for 5 min and resuspended in an equal volume of prewarmed TSB. HADA, $ZnCl_2$, and $MnCl_2$ were added to a final concentration of 100 mM, 0.5 mM, and 50 μM, respectively. The cultures were incubated at 37 °C in 5% CO_2, and samples were taken every 15 min for heat inactivation at 65 °C for 45 min. Cells were harvested by centrifugation at 20,000 × *g* for 2 min and washed once in PBS. Then, 100 μl cross-absorbed anti-serotype 2 CPS antiserum (SSI) was added at a 1:400 dilution, and the mixture was incubated on ice for 5 min. Cells were collected by centrifugation, washed once with PBS, and resuspended in 100 μl PBS. CPS was detected by adding goat anti-rabbit IgG conjugated with Alexa Fluor 647 (Thermo Fisher, A31573) at a 1:100 dilution and incubated on ice for 5 min. Labeled cells were washed with PBS and dispersed in 5 μl mounting medium (Thermo Fisher, S36936) and visualized using an IX81 microscope with a 100× oil immersion objective and a complementary metal oxide semiconductor (CMOS) camera (Hamamatsu, C11440). For SIM microscopy, acquisition was performed using a 100× CFI Plan Apo Lambda oil immersion objective with numerical aperture (1.45) mounted on a Nikon Eclipse Ti microscope, equipped with Yokogawa CSU-W1, Gataca Systems Live-SR module, and Photometrics Prime 95B scientific CMOS camera. Postprocessing of the acquired images was performed using the Live-SR software to obtain the super-resolution images. Images were processed by ImageJ and quantified by MicrobeJ version 5.12d (65) and Oufti version 1 (66). For the quantification of anti-CPS signal with MicrobeJ, the "Bacteria" and "Maxima" functions were used to detect and quantify the fluorescent signal and intensity. Under the "Bacteria" tab, "Medial Axis" was selected, and the thresholding function was adjusted accordingly to accurately detect the bacterial cells. To eliminate the detection of debris, "Area [μm^2]" was set to "0.15-max." The options "Exclude On Edges," "Shape descriptors," "Chain," and "Segmentation" were checked. "Foci" was selected to detect fluorescent signals. "Tolerance" and "Z-score" were adjusted accordingly to optimize the detection. Under the "association" tab, "Parent: Bacteria" and "Location" and "Outside" were selected. To quantify new PG incorporation, areas of bacteria were measured using the "Bacteria" function as described above using phase contrast images. The area of HADA was quantified using the "Maxima" function. Here, under the "association" tab, "Parent: Bacteria" was selected, and the "Location" and "Inside" were checked. Demographs were prepared by Oufti (66) using the demograph function under the tools and signal statistics tab. We set the parameters as follows: areaMin = 150, areaMax = 15,000, cellwidth = 20, wspringconst = 0.2, and split_threshold = 0.43. The incorporation of new PG was quantitated by measuring the HADA-labeled area over the total area of the cell using MicrobeJ (n = 20) (65). The multichannel 3D data were processed using Imaris 9.6.0 (Bitplane AG). The alignment between channels was performed using the channel shift function. The aligned data were then rendered in 3D and were used to prepare Movie S1.

Mass Spectrometry Analysis. Cells of the indicated strains were grown in 40 mL TSB and induced by adding Zn^{2+}. Twenty milliliters of OD_{600} 0.5 cultures was collected and harvested by centrifugation at 16,100 × *g* for 5 min at room temperature. Cells were washed three times with PBS, and bacterial pellets were resuspended in 1 mL PBS. Lipids were extracted by a modified Bligh and Dyer's method (67). A mixture of chloroform/methanol (1:2, vol:vol) was added, and samples were vortexed for 1 min and incubated with shaking at 6 °C for 4 h. Next, water and chloroform were added to the mixture and vortexed for 1 min. Phase separation was induced by centrifugation, and the lower organic layer was collected. The upper aqueous layer was re-extracted twice with chloroform. The organic layers were combined, dried with a vacuum concentrator (Labconco), and stored at −80 °C. Dried samples were reconstituted in a 1:1 mixture of chloroform/methanol, and the lipids were separated by liquid chromatography. Mass spectrometry and tandem mass spectrometry (MS/MS) analyses of lipids were performed using a SCIEX Triple-TOF 6600 Quadrupole Time-Of-Flight mass spectrometer in the negative electrospray ionization mode. For automated MS/MS analyses, the mass spectrometer was operated in the information-dependent acquisition mode with the top 20 ions selected per scan for fragmentation (collision energy: 65 V). Relative quantification of Und-P was based on area under the extracted ion chromatogram. Statistical analysis was conducted using a two-tailed Student's *t* test.

Data Availability. All study data are included in the article and/or supporting information.

ACKNOWLEDGMENTS. We thank Dr. Thomas G. Bernhardt for his support and advice on this work, Dr. Kimberly Kline for providing valuable feedback, Dr. Malcolm Winkler for the pneumococcal strains and the P-*erm* and P-*kan-rpsL*$^+$ cassettes, and Drs. Birgitta Henriques Normark and Staffan Normark for the helpful discussions and for providing strain TIGR4. We also thank Ms. Stella Lee Yue Ting for her assistance with immunofluorescent microscopy, Mr. Daniel Chua Chong Hin for constructing strain NUS0267, and Dr. Justin Zik for constructing NUS1085. We thank all members of the L.T.S. laboratory and the Bernhardt laboratory for the useful discussions. This work is supported by the National University of Singapore Start-up grant (NUHSRO/2017/070/SU/01 to L.-T.S.), the National Research Foundation Fellowship (NRFF11-2019-0005 to L.-T.S.), the NIH (R35 GM136365 to M.S.V.), and the Nanyang Assistant Professorship Award from Lee Kong Chian School of Medicine, Nanyang Technological University (NTU) (to X.L.G.).

1. C. Troeger *et al.*, Estimates of the global, regional, and national morbidity, mortality, and aetiologies of lower respiratory infections in 195 countries, 1990-2016: A systematic analysis for the Global Burden of Disease Study 2016. *Lancet Infect. Dis.* **18**, 1191–1210 (2018).
2. J. Yother, Capsules of *Streptococcus pneumoniae* and other bacteria: Paradigms for polysaccharide biosynthesis and regulation. *Annu. Rev. Microbiol.* **65**, 563–581 (2011).
3. K. A. Geno *et al.*, Pneumococcal capsules and their types: Past, present, and future. *Clin. Microbiol. Rev.* **28**, 871–899 (2015).
4. T. Su, *et al.*, Decoding capsule synthesis in *Streptococcus pneumoniae*. *FEMS Microbiol. Rev.* **44**, fuaa067 (2020).
5. J. C. Paton, C. Trappetti, *Streptococcus pneumoniae* capsular polysaccharide. *Microbiol. Spectr.* **7**, GPP3-0019-2018 (2019).
6. A. D. Magee, J. Yother, Requirement for capsule in colonization by *Streptococcus pneumoniae*. *Infect. Immun.* **69**, 3755–3761 (2001).
7. C. Hyams, E. Camberlein, J. M. Cohen, K. Bax, J. S. Brown, The *Streptococcus pneumoniae* capsule inhibits complement activity and neutrophil phagocytosis by multiple mechanisms. *Infect. Immun.* **78**, 704–715 (2010).
8. E. Mitsi *et al.*, Agglutination by anti-capsular polysaccharide antibody is associated with protection against experimental human pneumococcal carriage. *Mucosal Immunol.* **10**, 385–394 (2017).
9. A. J. van Tonder *et al.*, Putative novel *cps* loci in a large global collection of pneumococci. *Microb. Genom.* **5**, e000274 (2019).
10. J. D. Grabenstein, K. P. Klugman, A century of pneumococcal vaccination research in humans. *Clin. Microbiol. Infect.* **18** (suppl. 5), 15–24 (2012).
11. N. J. Croucher *et al.*, Rapid pneumococcal evolution in response to clinical interventions. *Science* **331**, 430–434 (2011).
12. M. G. Shainheit, M. Mulé, A. Camilli, The core promoter of the capsule operon of *Streptococcus pneumoniae* is necessary for colonization and invasive disease. *Infect. Immun.* **82**, 694–705 (2014).
13. Y. Kawai *et al.*, A widespread family of bacterial cell wall assembly proteins. *EMBO J.* **30**, 4931–4941 (2011).
14. Y. G. Chan, H. K. Kim, O. Schneewind, D. Missiakas, The capsular polysaccharide of *Staphylococcus aureus* is attached to peptidoglycan by the LytR-CpsA-Psr (LCP) family of enzymes. *J. Biol. Chem.* **289**, 15680–15690 (2014).
15. K. Schaefer, L. M. Matano, Y. Qiao, D. Kahne, S. Walker, In vitro reconstitution demonstrates the cell wall ligase activity of LCP proteins. *Nat. Chem. Biol.* **13**, 396–401 (2017).
16. C. Toniolo *et al.*, *Streptococcus agalactiae* capsule polymer length and attachment is determined by the proteins CpsABCD. *J. Biol. Chem.* **290**, 9521–9532 (2015).
17. M. H. Bender, R. T. Cartee, J. Yother, Positive correlation between tyrosine phosphorylation of CpsD and capsular polysaccharide production in *Streptococcus pneumoniae*. *J. Bacteriol.* **185**, 6057–6066 (2003).
18. T. R. Larson, J. Yother, *Streptococcus pneumoniae* capsular polysaccharide is linked to peptidoglycan via a direct glycosidic bond to β-D-*N*-acetylglucosamine. *Proc. Natl. Acad. Sci. U.S.A.* **114**, 5695–5700 (2017).
19. R. T. Cartee, W. T. Forsee, M. H. Bender, K. D. Ambrose, J. Yother, CpsE from type 2 *Streptococcus pneumoniae* catalyzes the reversible addition of glucose-1-phosphate to a polyprenyl phosphate acceptor, initiating type 2 capsule repeat unit formation. *J. Bacteriol.* **187**, 7425–7433 (2005).
20. G. Manat *et al.*, Deciphering the metabolism of undecaprenyl-phosphate: The bacterial cell-wall unit carrier at the membrane frontier. *Microb. Drug Resist.* **20**, 199–214 (2014).
21. B. Xayarath, J. Yother, Mutations blocking side chain assembly, polymerization, or transport of a Wzy-dependent *Streptococcus pneumoniae* capsule are lethal in the absence of suppressor mutations and can affect polymer transfer to the cell wall. *J. Bacteriol.* **189**, 3369–3381 (2007).
22. D. B. James, K. Gupta, J. R. Hauser, J. Yother, Biochemical activities of *Streptococcus pneumoniae* serotype 2 capsular glycosyltransferases and significance of suppressor mutations affecting the initiating glycosyltransferase Cps2E. *J. Bacteriol.* **195**, 5469–5478 (2013).
23. A. D. Ogunniyi, P. Giammarinaro, J. C. Paton, The genes encoding virulence-associated proteins and the capsule of *Streptococcus pneumoniae* are upregulated and differentially expressed in vivo. *Microbiology (Reading)* **148**, 2045–2053 (2002).
24. Z. Wen, Y. Liu, F. Qu, J. R. Zhang, Allelic variation of the capsule promoter diversifies encapsulation and virulence in *Streptococcus pneumoniae*. *Sci. Rep.* **6**, 30176 (2016).
25. A. S. Manso *et al.*, A random six-phase switch regulates pneumococcal virulence via global epigenetic changes. *Nat. Commun.* **5**, 5055 (2014).

26. J. Wang *et al.*, Regulation of pneumococcal epigenetic and colony phases by multiple two-component regulatory systems. *PLoS Pathog.* **16**, e1008417 (2020).
27. J. O. Kim, J. N. Weiser, Association of intrastrain phase variation in quantity of capsular polysaccharide and teichoic acid with the virulence of *Streptococcus pneumoniae*. *J. Infect. Dis.* **177**, 368–377 (1998).
28. J. Nourikyan *et al.*, Autophosphorylation of the bacterial tyrosine-kinase cpsd connects capsule synthesis with the cell cycle in *Streptococcus pneumoniae*. *PLoS Genet.* **11**, e1005518 (2015).
29. K. A. Geno, J. R. Hauser, K. Gupta, J. Yother, *Streptococcus pneumoniae* phosphotyrosine phosphatase CpsB and alterations in capsule production resulting from changes in oxygen availability. *J. Bacteriol.* **196**, 1992–2003 (2014).
30. M. X. Henriques, T. Rodrigues, M. Carido, L. Ferreira, S. R. Filipe, Synthesis of capsular polysaccharide at the division septum of *Streptococcus pneumoniae* is dependent on a bacterial tyrosine kinase. *Mol. Microbiol.* **82**, 515–534 (2011).
31. M. Rausch *et al.*, Coordination of capsule assembly and cell wall biosynthesis in *Staphylococcus aureus*. *Nat. Commun.* **10**, 1404 (2019).
32. T. van Opijnen, K. L. Bodi, A. Camilli, Tn-seq: High-throughput parallel sequencing for fitness and genetic interaction studies in microorganisms. *Nat. Methods* **6**, 767–772 (2009).
33. J. Neef, V. F. Andisi, K. S. Kim, O. P. Kuipers, J. J. E. Bijlsma, Deletion of a cation transporter promotes lysis in *Streptococcus pneumoniae*. *Infect. Immun.* **79**, 2314–2323 (2011).
34. J. K. Morona, R. Morona, J. C. Paton, Attachment of capsular polysaccharide to the cell wall of *Streptococcus pneumoniae* type 2 is required for invasive disease. *Proc. Natl. Acad. Sci. U.S.A.* **103**, 8505–8510 (2006).
35. D. Soulat *et al.*, *Staphylococcus aureus* operates protein-tyrosine phosphorylation through a specific mechanism. *J. Biol. Chem.* **281**, 14048–14056 (2006).
36. C. Whitfield, D. M. Williams, S. D. Kelly, Lipopolysaccharide O-antigens-bacterial glycans made to measure. *J. Biol. Chem.* **295**, 10593–10609 (2020).
37. R. Woodward *et al.*, In vitro bacterial polysaccharide biosynthesis: Defining the functions of Wzy and Wzz. *Nat. Chem. Biol.* **6**, 418–423 (2010).
38. W. P. Robins, S. M. Faruque, J. J. Mekalanos, Coupling mutagenesis and parallel deep sequencing to probe essential residues in a genome or gene. *Proc. Natl. Acad. Sci. U.S.A.* **110**, E848–E857 (2013).
39. B. Wiseman, R. G. Nitharwal, G. Widmalm, M. Högbom, Structure of a full-length bacterial polysaccharide co-polymerase. *Nat. Commun.* **12**, 369 (2021).
40. C. Mercy *et al.*, RocS drives chromosome segregation and nucleoid protection in *Streptococcus pneumoniae*. *Nat. Microbiol.* **4**, 1661–1670 (2019).
41. Y.-P. Hsu *et al.*, Full color palette of fluorescent d-amino acids for *in situ* labeling of bacterial cell walls. *Chem. Sci. (Camb.)* **8**, 6313–6321 (2017).
42. H. T. Tsui *et al.*, Pbp2x localizes separately from Pbp2b and other peptidoglycan synthesis proteins during later stages of cell division of *Streptococcus pneumoniae* D39. *Mol. Microbiol.* **94**, 21–40 (2014).
43. A. J. Perez *et al.*, Movement dynamics of divisome proteins and PBP2x:FtsW in cells of *Streptococcus pneumoniae*. *Proc. Natl. Acad. Sci. U.S.A.* **116**, 3211–3220 (2019).
44. A. K. Fenton, L. El Mortaji, D. T. Lau, D. Z. Rudner, T. G. Bernhardt, CozE is a member of the MreCD complex that directs cell elongation in *Streptococcus pneumoniae*. *Nat. Microbiol.* **2**, 16237 (2016).
45. M. El Ghachi, A. Bouhss, D. Blanot, D. Mengin-Lecreulx, The *bacA* gene of *Escherichia coli* encodes an undecaprenyl pyrophosphate phosphatase activity. *J. Biol. Chem.* **279**, 30106–30113 (2004).
46. O. Kocaoglu, H. C. Tsui, M. E. Winkler, E. E. Carlson, Profiling of β-lactam selectivity for penicillin-binding proteins in *Streptococcus pneumoniae* D39. *Antimicrob. Agents Chemother.* **59**, 3548–3555 (2015).
47. O. Kocaoglu *et al.*, Selective penicillin-binding protein imaging probes reveal substructure in bacterial cell division. *ACS Chem. Biol.* **7**, 1746–1753 (2012).
48. V. Olivares-Illana *et al.*, Structural basis for the regulation mechanism of the tyrosine kinase CapB from *Staphylococcus aureus*. *PLoS Biol.* **6**, e143 (2008).
49. N. Grossman *et al.*, Lipopolysaccharide size and distribution determine serum resistance in *Salmonella montevideo*. *J. Bacteriol.* **169**, 856–863 (1987).
50. K. A. Joiner, N. Grossman, M. Schmetz, L. Leive, C3 binds preferentially to long-chain lipopolysaccharide during alternative pathway activation by *Salmonella montevideo*. *J. Immunol.* **136**, 710–715 (1986).
51. E. Llobet, J. M. Tomás, J. A. Bengoechea, Capsule polysaccharide is a bacterial decoy for antimicrobial peptides. *Microbiology (Reading)* **154**, 3877–3886 (2008).
52. J. Fernebro *et al.*, Capsular expression in *Streptococcus pneumoniae* negatively affects spontaneous and antibiotic-induced lysis and contributes to antibiotic tolerance. *J. Infect. Dis.* **189**, 328–338 (2004).
53. C. C. Kietzman, G. Gao, B. Mann, L. Myers, E. I. Tuomanen, Dynamic capsule restructuring by the main pneumococcal autolysin LytA in response to the epithelium. *Nat. Commun.* **7**, 10859 (2016).
54. A. Pathak *et al.*, Factor H binding proteins protect division septa on encapsulated *Streptococcus pneumoniae* against complement C3b deposition and amplification. *Nat. Commun.* **9**, 3398 (2018).
55. G. Stefanetti, N. Okan, A. Fink, E. Gardner, D. L. Kasper, Glycoconjugate vaccine using a genetically modified O antigen induces protective antibodies to *Francisella tularensis*. *Proc. Natl. Acad. Sci. U.S.A.* **116**, 7062–7070 (2019).
56. R. Junges *et al.*, Markerless genome editing in competent Streptococci. *Methods Mol. Biol.* **1537**, 233–247 (2017).
57. Y. Li, C. M. Thompson, M. Lipsitch, A modified Janus cassette (Sweet Janus) to improve allelic replacement efficiency by high-stringency negative selection in *Streptococcus pneumoniae*. *PLoS One* **9**, e100510 (2014).
58. C. K. Sung, H. Li, J. P. Claverys, D. A. Morrison, An *rpsL* cassette, *janus*, for gene replacement through negative selection in *Streptococcus pneumoniae*. *Appl. Environ. Microbiol.* **67**, 5190–5196 (2001).
59. F. H. Ramírez-Guadiana, A. J. Meeske, X. Wang, C. D. A. Rodrigues, D. Z. Rudner, The *Bacillus subtilis* germinant receptor GerA triggers premature germination in response to morphological defects during sporulation. *Mol. Microbiol.* **105**, 689–704 (2017).
60. J. Flores-Kim, G. S. Dobihal, A. Fenton, D. Z. Rudner, T. G. Bernhardt, A switch in surface polymer biogenesis triggers growth-phase-dependent and antibiotic-induced bacteriolysis. *eLife* **8**, e44912 (2019).
61. B. E. Rued *et al.*, Suppression and synthetic-lethal genetic relationships of Δ*gpsB* mutations indicate that GpsB mediates protein phosphorylation and penicillin-binding protein interactions in *Streptococcus pneumoniae* D39. *Mol. Microbiol.* **103**, 931–957 (2017).
62. C. de Chiara, A. Pastore, Kaleidoscopic protein-protein interactions in the life and death of ataxin-1: New strategies against protein aggregation. *Trends Neurosci.* **37**, 211–218 (2014).
63. S. Zheng *et al.*, Structure and mutagenic analysis of the lipid II flippase MurJ from *Escherichia coli*. *Proc. Natl. Acad. Sci. U.S.A.* **115**, 6709–6714 (2018).
64. A. J. Meeske *et al.*, SEDS proteins are a widespread family of bacterial cell wall polymerases. *Nature* **537**, 634–638 (2016).
65. A. Ducret, E. M. Quardokus, Y. V. Brun, J. Microbe, MicrobeJ, a tool for high throughput bacterial cell detection and quantitative analysis. *Nat. Microbiol.* **1**, 16077 (2016).
66. A. Paintdakhi *et al.*, Oufti: An integrated software package for high-accuracy, high-throughput quantitative microscopy analysis. *Mol. Microbiol.* **99**, 767–777 (2016).
67. E. G. Bligh, W. J. Dyer, A rapid method of total lipid extraction and purification. *Can. J. Biochem. Physiol.* **37**, 911–917 (1959).